

A general method for determining the masses of semi-invisibly decaying particles at hadron colliders

Konstantin T. Matchev and Myeonghun Park
 Physics Department, University of Florida, Gainesville, FL 32611, USA
 (Dated: 27 December, 2010)

We present a general solution to the long standing problem of determining the masses of pair-produced, semi-invisibly decaying particles at hadron colliders. We define two new transverse kinematic variables, $M_{CT\perp}$ and $M_{CT\parallel}$, which are suitable one-dimensional projections of the contravariant mass M_{CT} . We derive analytical formulas for the boundaries of the kinematically allowed regions in the $(M_{CT\perp}, M_{CT\parallel})$ and $(M_{CT\perp}, M_{CT})$ parameter planes, and introduce suitable variables $D_{CT\parallel}$ and D_{CT} to measure the distance to those boundaries on an event per event basis. We show that the masses can be reliably extracted from the endpoint measurements of $M_{CT\perp}^{max}$ and D_{CT}^{min} (or $D_{CT\parallel}^{min}$). We illustrate our method with dilepton $t\bar{t}$ events at the LHC.

PACS numbers: 14.80.Ly, 12.60.Jv, 11.80.Cr

The ongoing run of the Large Hadron Collider (LHC) at CERN will finally provide the first glimpse of physics at the TeV scale. In large part, the excitement surrounding the LHC is fueled by the anticipation of the unknown: no one knows for sure where or how the first signal of new physics beyond the standard model (BSM) will show up. Yet, complementary and independent arguments from particle physics *and* astrophysics suggest that the best place to look for new physics is a channel with missing transverse energy \cancel{E}_T , caused by unseen new particles contributing to the dark matter of the Universe.

Unfortunately, the study of missing energy signatures poses a tremendous challenge at hadron colliders like the LHC. The first fundamental difficulty is related to the very nature of hadron colliders, where in each event the partonic center-of-mass energy \sqrt{s} and longitudinal momentum p_z of the initial state are unknown. To make matters worse, the lifetime of the dark matter particle is typically protected by a new parity symmetry, which guarantees that in every event the missing particles come in pairs, thus proliferating the number of unknown parameters describing the final state event kinematics.

The generic topology of a “new physics” \cancel{E}_T event is sketched in Fig. 1. Consider the *inclusive* production of an identical pair of new “parent” particles P . Each parent P decays semi-invisibly to a set V_i ($i = 1, 2$) of standard model (SM) particles, which are visible in the detector, and a dark matter particle C (from now on referred to as the “child”) which escapes detection. In general, the parent pair is accompanied by a number of additional “upstream” objects U (typically jets) with total transverse momentum \vec{U}_T . They may originate from various sources such as initial state radiation or decays of even heavier particles. We shall not be interested in the exact details of the physics responsible for U , adopting a fully inclusive approach to the production of the parents P . Given this general setup, the goal is to determine *independently* the mass M_p of the parent and the mass M_c of the child in terms of U , V_1 and V_2 .

In the past, several approaches to this problem have been proposed, but each has its own limitations. For example, the classic method of invariant mass endpoints [1, 2] only applies when the visible SM particles in V_i arise from a sufficiently long decay chain. Attempts at direct reconstruction [3] of the children momenta are again limited to long decay chains only. In this letter, we shall consider the extreme, most challenging example where each visible set V_i consists of a *single* SM particle of fixed mass m_i . A perfect testing ground for this scenario is provided by dilepton $t\bar{t}$ events (already observed at the LHC [4]) and we shall use that example in our numerical illustrations below. The role of the parent P (child C) will be played by the SM W -boson (SM neutrino), each V_i is a SM lepton (e or μ), while U is composed of the two b -jets from the top quark decays, plus any additional QCD jets from initial state radiation (ISR).

For such extremely short decay chains, the only viable alternative at the moment is provided by the methods based on the M_{T2} variable [5]. There, at least in principle, the individual masses M_p and M_c can be determined by observing a “kink” feature in the M_{T2} endpoint as a function of a hypothesized trial mass M_c for C [6], or by

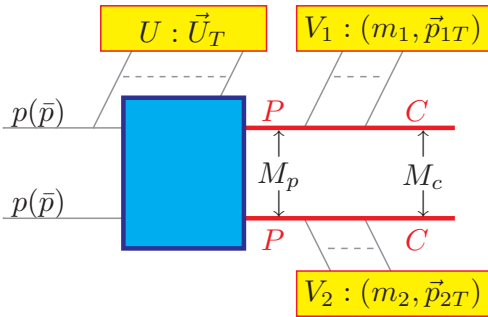


FIG. 1: The generic event topology under consideration. All particles visible in the detector are clustered into three groups: upstream objects U with total transverse momentum \vec{U}_T , and two composite visible particles V_i ($i = 1, 2$), each with invariant mass m_i and total transverse momentum \vec{p}_{iT} .

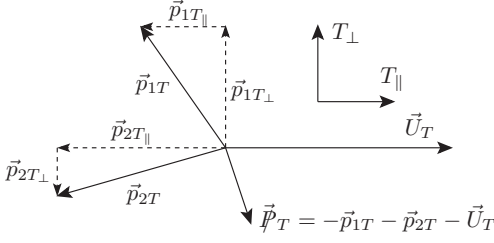


FIG. 2: Decomposition of the observed transverse momentum vectors from Fig. 1 in the transverse plane.

exploring the U_T dependence of the M_{T2} endpoint [7]. Compared to those M_{T2} approaches, our method here has two advantages. First, it is simpler – it uses only the observed objects U , V_1 and V_2 in the event and makes no reference to the missing particle kinematics (or mass). Second, it is more precise, since it utilizes the whole kinematic boundary of the relevant *two-dimensional* distribution and not just the kinematic endpoint of its *one-dimensional* projection. We proceed in three easy steps.

Step I. Orthogonal decomposition of the observed transverse momenta with respect to the \vec{U}_T direction. The Tevatron and LHC collaborations currently use fixed axes coordinate systems to describe their data. Instead, we propose to rotate the coordinate system from one event to another, so that the transverse axes are always aligned with the direction T_{\parallel} selected by the measured upstream transverse momentum vector \vec{U}_T and the direction T_{\perp} orthogonal to it (see Fig. 2). The visible transverse momentum vectors from Fig. 1 are then decomposed as

$$\vec{p}_{iT_{\parallel}} \equiv \frac{1}{U_T^2} (\vec{p}_{iT} \cdot \vec{U}_T) \vec{U}_T, \quad (1)$$

$$\vec{p}_{iT_{\perp}} \equiv \vec{p}_{iT} - \vec{p}_{iT_{\parallel}} = \frac{1}{U_T^2} \vec{U}_T \times (\vec{p}_{iT} \times \vec{U}_T). \quad (2)$$

Step II. Constructing the transverse and longitudinal contranverse masses $M_{CT_{\perp}}$ and $M_{CT_{\parallel}}$. Our starting point is the original contranverse mass variable [8]

$$M_{CT} = \sqrt{m_1^2 + m_2^2 + 2(e_{1T}e_{2T} + \vec{p}_{1T} \cdot \vec{p}_{2T})}, \quad (3)$$

where e_{iT} is the “transverse energy” of V_i

$$e_{iT} = \sqrt{m_i^2 + |\vec{p}_{iT}|^2}. \quad (4)$$

For events with $U_T = 0$, M_{CT} has an upper endpoint which is insensitive to the unknown \sqrt{s} , providing one relation among M_p and M_c [8, 9]

$$M_{CT}^{max}(U_T = 0) = \sqrt{m_1^2 + m_2^2 + 2m_1m_2 \cosh(\zeta_1 + \zeta_2)}, \quad (5)$$

where

$$\sinh \zeta_i \equiv \frac{\lambda^{\frac{1}{2}}(M_p^2, M_c^2, m_i^2)}{2M_p m_i}, \quad (6)$$

$$\lambda(x, y, z) \equiv x^2 + y^2 + z^2 - 2xy - 2xz - 2yz. \quad (7)$$

Unfortunately, the $U_T = 0$ limit is not particularly interesting at hadron colliders (especially for inclusive studies), since a significant amount of upstream U_T is typically generated by ISR (and other) jets. One possible fix is to use all events, but modify the definition (3) to approximately compensate for the transverse \vec{U}_T boost [9]. One then recovers a distribution whose endpoint is still given by (5). Alternatively, one could stick to the original M_{CT} variable, and simply account for the U_T dependence of its endpoint as

$$M_{CT}^{max}(U_T) = \sqrt{m_1^2 + m_2^2 + 2m_1m_2 \cosh(2\eta + \zeta_1 + \zeta_2)} \quad (8)$$

where ζ_i were already defined in (6), and

$$\sinh \eta \equiv \frac{U_T}{2M_p}, \quad \cosh \eta \equiv \sqrt{1 + \frac{U_T^2}{4M_p^2}}. \quad (9)$$

Our approach here is to utilize the one-dimensional projections from eqs. (1,2) and construct one-dimensional analogues of the M_{CT} variable

$$M_{CT_{\perp}} \equiv \sqrt{m_1^2 + m_2^2 + 2(e_{1T_{\perp}}e_{2T_{\perp}} + \vec{p}_{1T_{\perp}} \cdot \vec{p}_{2T_{\perp}})}, \quad (10)$$

$$M_{CT_{\parallel}} \equiv \sqrt{m_1^2 + m_2^2 + 2(e_{1T_{\parallel}}e_{2T_{\parallel}} + \vec{p}_{1T_{\parallel}} \cdot \vec{p}_{2T_{\parallel}})}, \quad (11)$$

where the corresponding “transverse energies” are

$$e_{iT_{\perp}} \equiv \sqrt{m_i^2 + |\vec{p}_{iT_{\perp}}|^2}, \quad e_{iT_{\parallel}} \equiv \sqrt{m_i^2 + |\vec{p}_{iT_{\parallel}}|^2}. \quad (12)$$

The benefit of the decomposition (10,11) is that one gets “two for the price of one”, i.e. two independent and complementary variables instead of the single variable (3).

The variable $M_{CT_{\perp}}$ in particular is very useful for our purposes. To illustrate the basic idea, it is sufficient to consider the most common case, where V_i is approximately massless ($m_i = 0$), as the leptons in our $t\bar{t}$ example. A crucial property of $M_{CT_{\perp}}$ is that its endpoint is independent of U_T :

$$M_{CT_{\perp}}^{max} = \frac{M_p^2 - M_c^2}{M_p}, \quad \forall U_T. \quad (13)$$

In fact the whole $M_{CT_{\perp}}$ distribution is insensitive to U_T :

$$\frac{dN}{dM_{CT_{\perp}}} = N_{0_{\perp}} \delta(M_{CT_{\perp}}) + (N_{tot} - N_{0_{\perp}}) \frac{d\bar{N}}{dM_{CT_{\perp}}}, \quad (14)$$

where $N_{0_{\perp}}$ is the number of events in the zero bin $M_{CT_{\perp}} = 0$. Using phase space kinematics, we find that the shape of the remaining (unit-normalized) zero-bin-subtracted distribution is simply given by

$$\frac{d\bar{N}}{d\hat{M}_{CT_{\perp}}} \equiv -4 \hat{M}_{CT_{\perp}} \ln \hat{M}_{CT_{\perp}} \quad (15)$$

in terms of the unit-normalized $M_{CT_{\perp}}$ variable

$$\hat{M}_{CT_{\perp}} \equiv \frac{M_{CT_{\perp}}}{M_{CT_{\perp}}^{max}}. \quad (16)$$

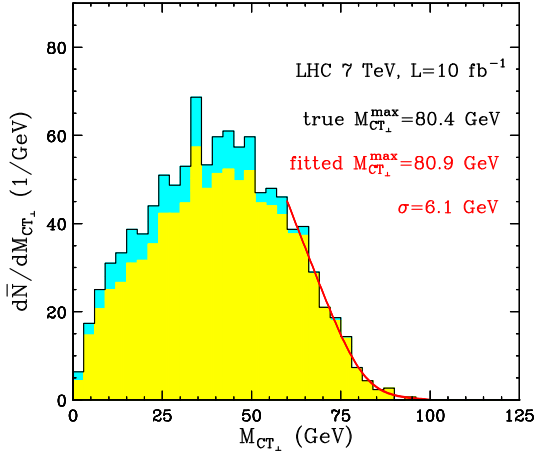


FIG. 3: Zero-bin subtracted M_{CT_\perp} distribution after cuts, for $t\bar{t}$ dilepton events. The yellow (lower) portion is our signal, while the blue (upper) portion shows $t\bar{t}$ combinatorial background with isolated leptons arising from τ or b decays.

The observable M_{CT_\perp} distribution for our $t\bar{t}$ example is shown in Fig. 3, for 10 fb^{-1} of LHC data at 7 TeV. Events were generated with PYTHIA [10] and processed with the PGS detector simulator [11]. We apply standard background rejection cuts as follows [4]: we require two isolated, opposite sign leptons with $p_{iT} > 20 \text{ GeV}$, $m_{\ell+\ell-} > 12 \text{ GeV}$, and passing a Z -veto $|m_{\ell+\ell-} - M_Z| > 15 \text{ GeV}$; at least two central jets with $p_T > 30 \text{ GeV}$ and $|\eta| < 2.4$; and a \cancel{E}_T cut of $\cancel{E}_T > 30 \text{ GeV}$ ($\cancel{E}_T > 20 \text{ GeV}$) for events with same flavor (opposite flavor) leptons. We also demand at least two b -tagged jets, assuming a flat b -tagging efficiency of 60%. With those cuts, the SM background from other processes is negligible [4].

Fig. 3 demonstrates that the M_{CT_\perp} endpoint can be measured quite well. Since the theoretically predicted shape (15) is distorted by the cuts, we use a linear slope with Gaussian smearing, and fit for the endpoint and the resolution parameter. We find $M_{CT_\perp}^{max} = 80.9 \text{ GeV}$ (compare to the true value $M_{CT_\perp}^{max} = 80.4 \text{ GeV}$), which gives one constraint (13) among M_p and M_c . At this point, a second, independent constraint can in principle be obtained from an analogous measurement of the M_{CT}^{max} endpoint (8) at a fixed value of U_T (resulting in loss in statistics), after which the two masses can be found from

$$M_p = \frac{U_T M_{CT}^{max}(U_T) M_{CT_\perp}^{max}}{(M_{CT}^{max}(U_T))^2 - (M_{CT_\perp}^{max})^2}, \quad (17)$$

$$M_c = \sqrt{M_p (M_p - M_{CT_\perp}^{max})}. \quad (18)$$

However, the orthogonal decomposition (10,11) offers an other approach, which we pursue in the last step.

Step III. Fitting to kinematic boundary lines. It is known that two-dimensional correlation plots reveal a lot more information than one-dimensional projected histograms [2, 12]. To this end, consider the scatter plot of M_{CT_\perp} vs M_{CT_\parallel} in Fig. 4(a), where for illustration we

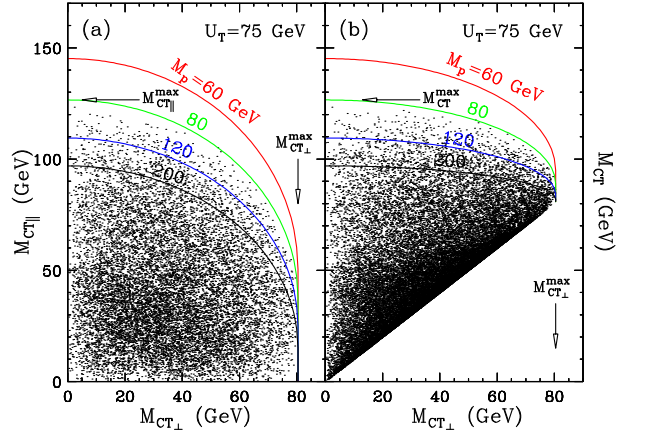


FIG. 4: Scatter plots of (a) M_{CT_\perp} versus M_{CT_\parallel} and (b) M_{CT_\perp} versus M_{CT} , for a fixed representative value $U_T = 75 \text{ GeV}$. The solid lines show the corresponding boundaries defined in (20) and (23), for the correct value of $M_{CT_\perp}^{max}$ and several different values of M_p as shown.

used 10,000 events at the parton level. For a given value of M_{CT_\perp} , the allowed values of M_{CT_\parallel} are bounded by

$$M_{CT_\parallel}^{(lo)}(M_{CT_\perp}) \leq M_{CT_\parallel} \leq M_{CT_\parallel}^{(hi)}(M_{CT_\perp}), \quad (19)$$

where $M_{CT_\parallel}^{(lo)}(M_{CT_\perp}) = 0$ and

$$M_{CT_\parallel}^{(hi)}(M_{CT_\perp}) = M_{CT_\perp}^{max} \left(\sqrt{1 - \hat{M}_{CT_\perp}^2} \cosh \eta + \sinh \eta \right). \quad (20)$$

Fig. 4(a) reveals that the endpoint $M_{CT_\parallel}^{max}$ of the one-dimensional M_{CT_\parallel} distribution is obtained at $M_{CT_\perp} = 0$

$$\begin{aligned} M_{CT_\parallel}^{max} &= M_{CT_\parallel}^{(hi)}(0) = M_{CT_\perp}^{max} (\cosh \eta + \sinh \eta) \\ &= \frac{1}{2} \left(1 - \frac{M_c^2}{M_p^2} \right) \left(\sqrt{4M_p^2 + U_T^2} + U_T \right). \end{aligned} \quad (21)$$

Notice that events in the zero bins $M_{CT_\perp} = 0$ and $M_{CT_\parallel} = 0$ fall on one of the axes and cannot be distinguished on the plot.

Now consider the scatter plot of M_{CT_\perp} vs M_{CT} shown in Fig. 4(b). M_{CT} is similarly bounded by

$$M_{CT}^{(lo)}(M_{CT_\perp}) \leq M_{CT} \leq M_{CT}^{(hi)}(M_{CT_\perp}), \quad (22)$$

where this time $M_{CT}^{(lo)}(M_{CT_\perp}) = M_{CT_\perp}$ and

$$M_{CT}^{(hi)}(M_{CT_\perp}) = M_{CT_\perp}^{max} \left(\cosh \eta + \sqrt{1 - \hat{M}_{CT_\perp}^2} \sinh \eta \right). \quad (23)$$

We see that the endpoint M_{CT}^{max} of the one-dimensional M_{CT} distribution is also obtained for $M_{CT_\perp} = 0$:

$$M_{CT}^{max} = M_{CT}^{(hi)}(0) = M_{CT_\perp}^{max} (\cosh \eta + \sinh \eta) = M_{CT_\parallel}^{max}. \quad (24)$$

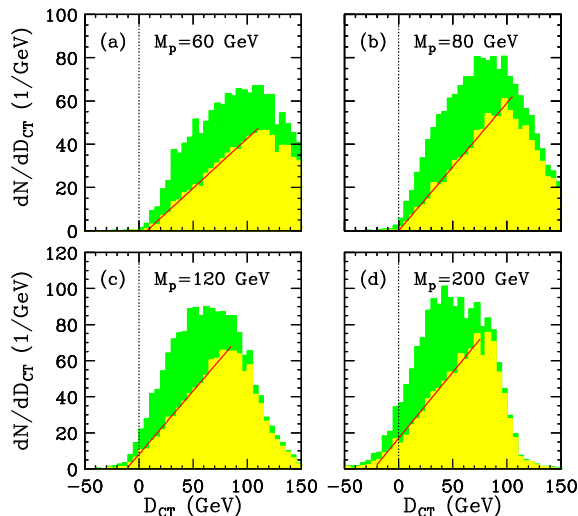


FIG. 5: D_{CT} distributions for four different values of M_p (and M_c given from (18)). The yellow (light shaded) histograms use only events in the zero bin $M_{CT\perp} = 0$. The red solid lines show linear binned maximum likelihood fits.

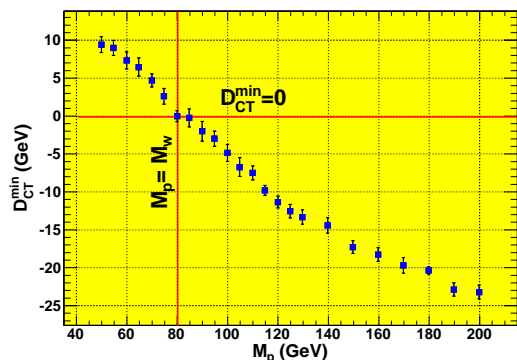


FIG. 6: Fitted values of D_{CT}^{min} as a function of M_p .

Fig. 4 reveals a conceptual problem with one-

dimensional projections. While *all* points in the vicinity of the boundary lines (20) and (23) are sensitive to the masses, the $M_{CT\perp}^{max}$ endpoint is extracted mostly from events with $M_{CT\perp} \sim M_{CT\perp}^{max}$, while the $M_{CT\parallel}^{max}$ and M_{CT}^{max} endpoints are extracted mostly from the events with $M_{CT\perp} \sim 0$. The events near the boundary, but with *intermediate* values of $M_{CT\perp}$, will not enter efficiently either one of these endpoint determinations.

So how can one do better, given the knowledge of the boundary line (23)? In the spirit of [13], we define the signed distance to the corresponding boundary, e.g.

$$D_{CT}(M_p, M_c) \equiv M_{CT}^{(hi)}(M_{CT\perp}, U_T, M_p, M_c) - M_{CT}$$

and similarly for $D_{CT\parallel}$. The key property of this variable is that for the correct values of M_p and M_c , its lower endpoint D_{CT}^{min} is exactly zero (see Fig. 5(b)):

$$D_{CT}^{min}(M_p, M_c) = 0. \quad (25)$$

In that case the boundary line provides a perfectly snug fit to the scatter plot — notice the green boundary line marked “80” in Fig. 4(b). While in general eq. (25) represents a two-dimensional fit to M_p and M_c , in practice one can already use the $M_{CT\perp}^{max}$ measurement to reduce the problem to a single degree of freedom, e.g. the parent mass M_p , as presented in Figs. 4 and 5. We see that the correct parent mass $M_p = 80$ GeV provides a perfect envelope, for which $D_{CT}^{min} = 0$. If, on the other hand, M_p is too low, a gap develops between the outlying points in the scatter plot and their expected boundary, which results in $D_{CT}^{min} > 0$. Conversely, if M_p is too high, some of the outlying points from the scatter plot fall outside the boundary and have $D_{CT} < 0$, leading to $D_{CT}^{min} < 0$, as seen in Fig. 5(c,d). The resulting fit for D_{CT}^{min} as a function of M_p from our PGS data sample is shown in Fig. 6, which suggests that a W mass measurement at the level of a few percent might be viable.

Acknowledgments. This work is supported in part by a US Department of Energy grant DE-FG02-97ER41029.

-
- [1] I. Hinchliffe *et al.*, Phys. Rev. D **55**, 5520 (1997); B. C. Allanach *et al.*, JHEP **0009**, 004 (2000); B. K. Gjelsten, D. J. Miller and P. Osland, JHEP **0412**, 003 (2004).
[2] K. T. Matchev, F. Moortgat, L. Pape and M. Park, JHEP **0908**, 104 (2009).
[3] K. Kawagoe, M. M. Nojiri and G. Polesello, Phys. Rev. D **71**, 035008 (2005); H. C. Cheng *et al.*, Phys. Rev. Lett. **100**, 252001 (2008).
[4] V. Khachatryan *et al.* [CMS Collaboration], arXiv:1010.5994 [hep-ex].
[5] C. G. Lester and D. J. Summers, Phys. Lett. B **463**, 99 (1999); A. Barr, C. Lester and P. Stephens, J. Phys. G **29**, 2343 (2003).
[6] A. J. Barr, B. Gripaios and C. G. Lester, JHEP **0802**, 014 (2008); M. Burns, K. Kong, K. T. Matchev and M. Park, JHEP **0903**, 143 (2009).
[7] K. T. Matchev, F. Moortgat, L. Pape and M. Park, Phys. Rev. D **82**, 077701 (2010); P. Konar, K. Kong, K. T. Matchev and M. Park, Phys. Rev. Lett. **105**, 051802 (2010).
[8] D. R. Tovey, JHEP **0804**, 034 (2008).
[9] G. Polesello and D. R. Tovey, JHEP **1003**, 030 (2010).
[10] T. Sjostrand, S. Mrenna and P. Skands, JHEP **0605**, 026 (2006).
[11] <http://www.physics.ucdavis.edu/~conway/research/software/pgs/pgs4-general.htm>
[12] D. Costanzo and D. R. Tovey, JHEP **0904**, 084 (2009); M. Burns, K. T. Matchev and M. Park, JHEP **0905**, 094 (2009).
[13] I. W. Kim, Phys. Rev. Lett. **104**, 081601 (2010).